ECE 445

SENIOR DESIGN LABORATORY

FINAL REPORT

Mobile eVTOL Handling and Docking Platform

Author Information

HAOWEN CHEN (3220110679)
RUILING XU (3220115546)
SHU YANG (3220110895)
YUCHEN ZHANG (3220111924)

Supervisor: Meng Zhang
TA: Kang Tan

May 17, 2026

Abstract

This report documents the design, implementation, and verification of the Mobile eVTOL Handling and Docking Platform, a prototype ground vehicle that addresses the manual ground-handling bottleneck in urban vertiport operations. The platform integrates a single-stage scissor lift, rotary deployable side wings, a four-wheel differential-drive chassis, and a Bluetooth Low Energy (BLE) remote-control link operated through a custom iOS application. A dedicated L293D-based motor driver printed circuit board (PCB) controls the linear actuator with separated 5 V logic and 7.4 V motor power rails. Bench verification confirmed correct H-bridge output states ($+7.3$ V forward, -7.2 V reverse, 0 V stop). Mechanical testing demonstrated a 93 mm support-plate stroke under a 500 g payload; the required 60 mm rise was reached within a conservative 15.5 s equivalent time, and the stop-command braking distance was 2.2–3.0 cm across twelve trials, both within the 60 mm/20 s and 5 cm requirements. link remained stable to 60 m indoors with command latency under 0.3 s.

Contents

1 Introduction

1.1 Background and Motivation

The rapid growth of the low-altitude economy has positioned eVTOL aircraft as a practical solution for urban air mobility [1], [2]. As vertiport operations scale up, ground handling becomes a critical bottleneck: aircraft must be repositioned between landing pads, charging bays, and maintenance lanes on tight turnaround schedules. Current practice relies on manual dollies and ad-hoc lift jacks, which are slow, labor-intensive, and risk structural overload on the airframe. A self-propelled platform capable of approaching, lifting, and transporting an eVTOL under remote command would directly address this gap.

To meet this need, we developed the **Mobile eVTOL Handling and Docking Platform**, a ground vehicle integrating a scissor lift, rotary deployable side wings, a four-wheel differential-drive chassis, a custom L293D-based actuator driver PCB, and a Bluetooth Low Energy (BLE) remote control link operated through a custom iOS application into a single operable prototype.

1.2 Final Solution Overview

The platform is shown in Figure 1, with key subsystems labeled in the CAD view: the scissor lift on the upper deck, the rotary side wings for lateral load spreading, the onboard electronics bay housing the Arduino Mega 2560, the custom L293D actuator driver PCB and the HC-08 BLE module, and four rubber-wheel TT gear motors at the chassis corners.

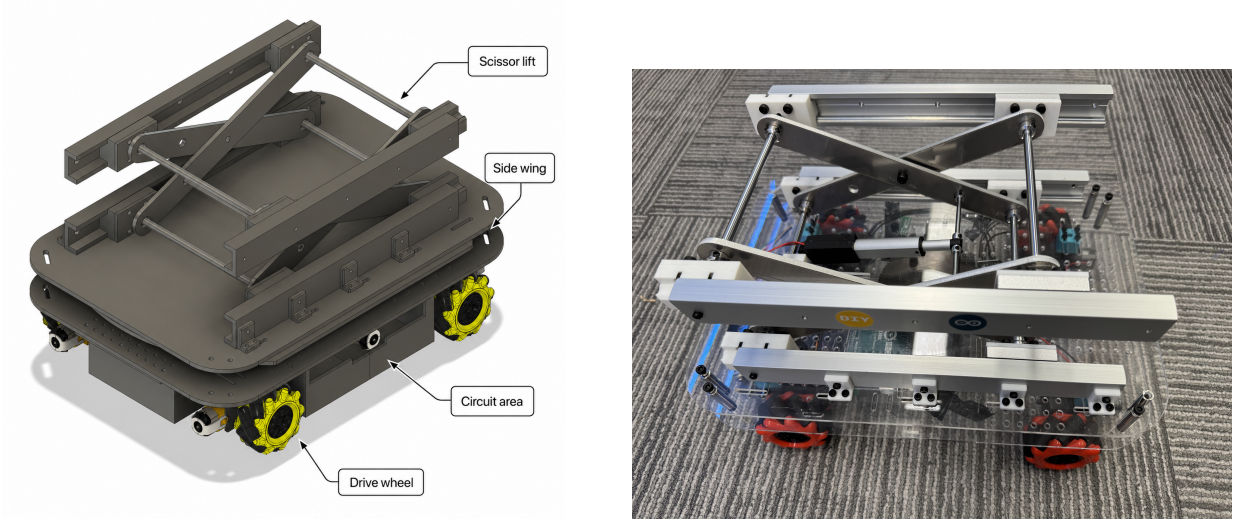

(a) Overall CAD model (b) Physical assembly

Figure 1: The Mobile eVTOL Handling and Docking Platform.

1.3 High-Level Requirements

Three high-level functionalities drive the prototype design. Each maps directly to a ground-handling task that a manual dolly cannot perform unsupervised, and each is verified quantitatively in Section 4 and Appendix A.

1. **Mechanical actuation.** The scissor lift shall raise a minimum 300 g prototype payload through at least 60 mm of vertical travel within 20 s, and the chassis shall stop within 5 cm after a stop command. This requirement underpins the platform's core ground-handling function: lifting an eVTOL clear of the landing pad surface and bringing it to rest at a predictable position so that handlers or downstream automation can engage the airframe safely.
2. **Electronic control.** The custom L293D-based actuator driver PCB shall produce forward, reverse, and stop output states ($|V_{\mathrm{OUT1}} - V_{\mathrm{OUT2}}| \geq 7.0$ V active, within ± 0.2 V of zero in stop) from logic-level Arduino inputs, with separated 5 V logic and 7.4 V motor rails sharing a common ground. This requirement enables deterministic, supervised actuator control without the noise problems documented in Section 2.1, and is a prerequisite for any eventual closed-loop lift control.
3. **Wireless link.** The HC-08 BLE module shall maintain a stable indoor connection beyond 10 m and deliver each command with an operator-visible response within 0.3 s. This requirement supports the platform's core operational concept: a single ground operator commanding the lift, wing-deploy, and drive functions from outside the rotor-downwash zone of the eVTOL, which is impossible with the manual dollies that motivate the project.

1.4 Subsystem Overview

The platform comprises three subsystems, shown in Figure 2. The **Remote Control System** consists of the iOS *eVTOL Control* app and the HC-08 BLE module, which forwards single-byte command opcodes to the Arduino over UART at 9600 baud. The **Onboard Electronic Control System** centers on the Arduino Mega 2560, which runs a safety supervisor and dispatches PWM signals to the wheel motor drivers and direction enables to the dedicated L293D actuator PCB; two separate 7.4 V packs power the lift and propulsion paths, sharing a common ground with the 5 V logic rail. The **Mechanical System** converts these outputs into physical motion: the scissor lift raises the support plate, the rotary side wings extend the load footprint, and the four TT gear motors drive the chassis.

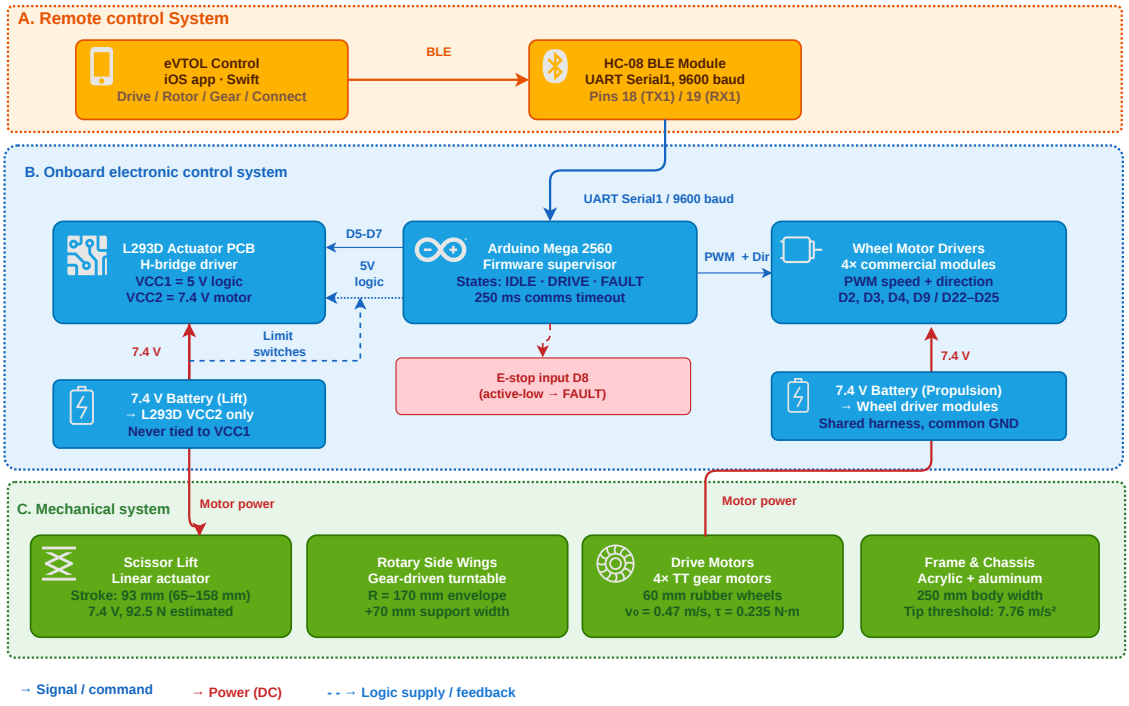

Figure 2: Top-level system architecture of the Mobile eVTOL Handling and Docking Platform.

2 Design Procedure

The design procedure combined first-principles analysis with CAD-based geometric verification and bench-level electrical prototyping. Three sets of design tools were applied. Mechanical sizing used closed-form kinematic and force-balance equations: the scissor linkage was modeled through the actuator-length relation (Eq. (4)), the velocity ratio (Eq. (6)), and the virtual-work load expression (Eq. (7)); the propulsion base was sized through the wheel-speed and wheel-force conversions (Eq. (1)–(2)); and stability was checked through the tipping-acceleration estimate (Eq. (9)). These analytical sweeps were implemented in MATLAB to generate the height-and-payload curves shown later in Figure 6. Mechanical geometry, interference, and assembly were validated in Fusion 360 CAD before fabrication. The electronic subsystem followed the standard L293D H-bridge form—a four-input, two-output driver with separated logic and motor supplies—laid out as a custom PCB in JLCEDA and fabricated through JLCPCB, then verified on the bench with a dual-rail supply and oscilloscope before system integration. The wireless link reused the HC-08 BLE module's default UART-bridge mode at 9600 baud, with command framing defined in the custom iOS application rather than at the hardware layer.

Several design decisions evolved during implementation as practical constraints emerged. Table 1 summarizes the key alternatives considered and the rationale behind each final choice.

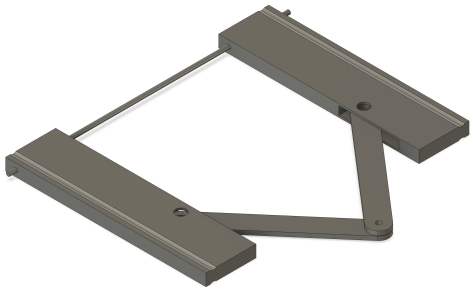

Figure 3: The initial linear-slider side-wing concept, later abandoned for the rotary design.

Table 1: Design alternatives considered and final decisions.

Issue	**Alternatives**	**Decision**	**Rationale**
Vertical lift mechanism	Scissor lift vs. vertical rail vs. direct jack	Scissor lift	Favorable force-to-stroke ratio within the compact chassis footprint, self-locks under load when unpowered, and accommodates the linear actuator attachment geometry derived in Section 3.1.
Lateral support	Rotary side wings vs. linear sliding wings vs. fixed wide platform	Rotary side wings	Eliminates the long exposed linear rails in Figure 3, which would have introduced asymmetric left/right deployment and a multi-DOF mechanism with amplified tolerance stack-up. A gear-driven turntable collapses each side to one DOF.
Wireless communication	Infrared vs. Bluetooth (HC-08)	HC-08 BLE	Infrared requires line-of-sight and has limited range; HC-08 provides reliable indoor range well beyond 10 m, integrates directly with `Serial1` on the Mega at 9600 baud, and supports a custom iOS app without additional hardware.
Ground mobility	Differential drive vs. omnidirectional vs. manual push	Differential drive	Requires only four standard TT gear motors and a straightforward PWM control path; omnidirectional wheels add mechanical complexity, and manual push removes remote-control capability entirely.
Power architecture	Single shared battery vs. isolated dual battery	Isolated dual supply	Separated 5 V logic and 7.4 V motor rails avoid injecting motor switching noise into the microcontroller and HC-08, and protect the Arduino and L293D VCC1 from the higher motor voltage (Section 3.2.1).

2.1 Design Issues and Corrective Actions

Three design issues required corrective action during implementation. Table 2 summarizes each issue, the triggering evidence, the corrective action, and the verified outcome.

Table 2: Design issues encountered and corrective actions taken.

Issue	**Evidence**	**Corrective action**	**Outcome**
Linear side-wing mechanism asymmetric and complex	Left and right linear stages required independent drives and developed unequal extension under simultaneous command; two rails, two carriages, two end stops, and two drive trains per side produced a tolerance stack-up amplifying tip errors.	Replaced with rotary turntable wings driven by a single pinion-and-gear stage about a vertical axis (Figure 7); each wing reduced to one DOF, two sides symmetric by construction.	70 mm support-width increase with no observed asymmetry; no exposed rails; repeatable across bench cycles.
Single-supply motor noise corrupted Arduino logic	Sharing one 7.4 V LiPo across Arduino, HC-08, and a TT motor caused HC-08 BLE dropouts in 4 of 10 startup trials and occasional Mega resets, with $\sim$0.6 V dips on the 5 V rail at motor commutation.	Split into dual-rail architecture (Table 5): dedicated 7.4 V lift pack, separate 7.4 V wheel pack, Arduino 5 V isolated for HC-08 and L293D VCC1, single common ground.	5 V rail noise below 50 mV; no further BLE dropouts or Mega resets.
L293D overcurrent at 12 V drive	Bench tests at 12 V produced 0.78 A peak during direction reversal, exceeding the L293D 600 mA per-channel rating.	Dropped actuator supply to 7.4 V; effective force scales to 92.5 N per Eq. (7), keeping the IC in safe operating area.	Practical payload envelope 0.52–0.70 kg still covers the 300–500 g range; no thermal shutdown observed.

3 Design Details

3.1 Mechanical System

The mechanical system provides the prototype load path, vertical motion, lateral support envelope, and ground mobility. It consists of a four-wheel propulsion base, a single-stage scissor lift, rotary side wings, and a frame sized for the 300–500 g payload tests. Figure 1 shows the CAD and assembled hardware.

The selected architecture was chosen over narrower two-wheel drive, vertical-rail lift, and linear side-wing concepts because the four-corner wheel layout increases the support polygon, the scissor lift provides the required vertical stroke within the available actuator range, and rotary wings avoid exposed long sliding rails. The calculations below therefore focus on the mechanical limits that govern the verified prototype behavior: wheel force, lift stroke, payload capacity, and braking stability.

3.1.1 Propulsion Subsystem

The propulsion base uses four TT gear motors near the chassis corners, each driving a 60 mm rubber-contact wheel (Figure 4). The corner wheel placement gives a wide support polygon and a short load path into the base plate, which is preferable for the stop-command tests in Section 4.1.

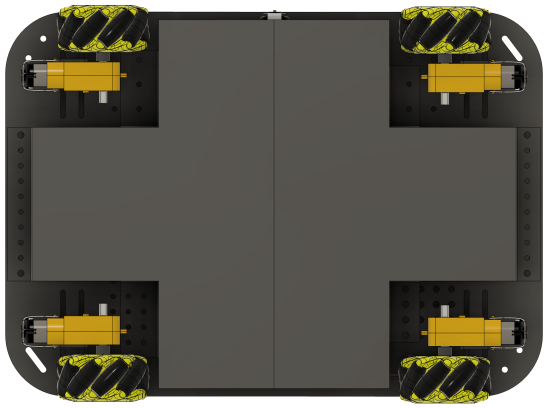

Figure 4: Bottom CAD view of the propulsion layout with four TT gear motors and corner wheel contact points.

For first-order sizing, the TT motor torque is $\tau_m = 2.4\ \mathrm{kg \cdot cm} = 0.235\ \mathrm{N \cdot m}$, the wheel radius is $r = 30$ mm, and the no-load speed is $n = 150$ rpm. These values give

$$v_0 = \frac{n}{60}(2\pi r) = 0.471\ \mathrm{m/s}, \tag{1}$$

$$F_{\mathrm{wheel}} = \frac{\tau_m}{r} = 7.85\ \mathrm{N}. \tag{2}$$

The four wheels therefore provide about 31.4 N before losses. For a 2.5 kg prototype-plus-payload estimate and $C_{rr} = 0.02$, the rolling resistance is only

$$F_{rr} = C_{rr} mg = 0.02(2.5)(9.81) = 0.49 \text{ N}, \tag{3}$$

which is much smaller than the available wheel force. The propulsion design is therefore not limited by steady rolling resistance; the relevant mechanical verification is repeatable stopping within 5 cm after a stop command.

3.1.2 Scissor Lift Subsystem

The lifting stage is a single-stage scissor mechanism built from two parallel X-linkages. One side is modeled as a planar scissor because both sides share the same geometry and are coupled by the top plate. Figure 5 shows the expanded and compressed prototype states.

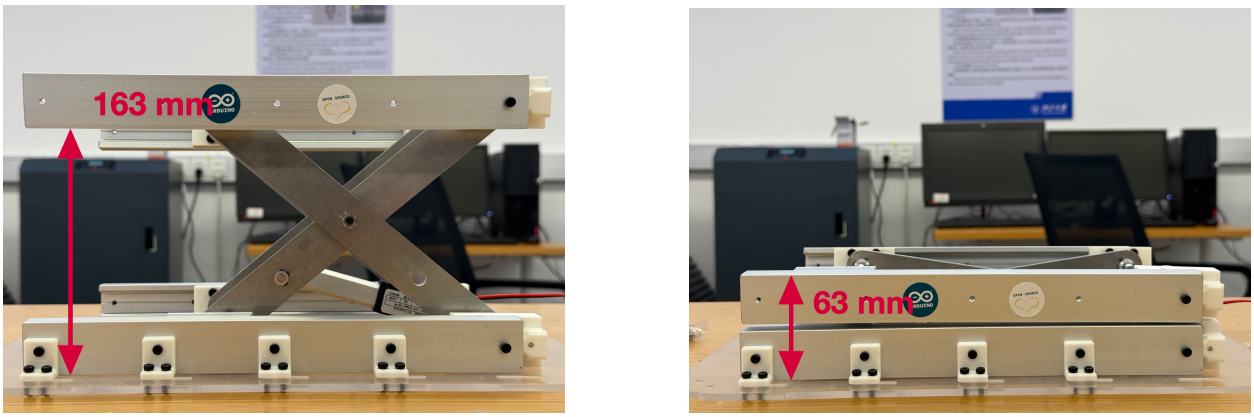

(a) Prototype expanded

(b) Prototype compressed

Figure 5: Scissor lift geometry and prototype states.

Each X-link has hole-to-hole length $L = 203$ mm. With horizontal span x, vertical joint separation H, and the actuator attached at one quarter of the link length, the geometry reduces to

$$x^2 + H^2 = L^2, \qquad l^2 = \frac{9L^2}{16} - \frac{H^2}{2}, \qquad H = \sqrt{\frac{9L^2}{8} - 2l^2}. \tag{4}$$

Rail clearance prevents full collapse. With $H_{\min} = 28$ mm, the lower-position actuator length is 150.96 mm; at $l_{\min} = 107.5$ mm, the model predicts $H_{\text{top}} = 152.47$ mm. The ideal joint-center travel is therefore

$$\Delta H = 152.47 - 28 = 124.47 \text{ mm}. \tag{5}$$

The assembled prototype measured 65–158 mm at the support plate, or 93 mm of usable plate travel. The difference from the pin-center model is due to rail offsets, brackets, plate thickness, and clearance.

Differentiating Equation (4) gives the vertical velocity ratio

$$|v_H| = \frac{2l}{H} |v_l| . \tag{6}$$

At the 7.4 V prototype supply, the actuator speed estimate is 2.47 mm/s. The mechanism moves faster near the lower position and more slowly near the top, where the force advantage is higher.

Load capacity is estimated by virtual work:

$$W = F_{\text{act}} \left| \frac{dl}{dH} \right| = F_{\text{act}} \frac{H}{2l}. \tag{7}$$

The 150 N actuator rating scales to $F_{7.4V} = 92.5$ N at the prototype supply. Equation (7) predicts an ideal payload of 0.87 kg at the lower position and 6.69 kg near the top. With $\eta = 0.6$–0.8 for friction and alignment loss, the practical full-stroke lower-position capacity is approximately 0.52–0.70 kg. This places the 300 g requirement inside the design envelope and makes the 500 g verification load a useful prototype stress case. Figure 6 plots the calculated height and payload capacity.

To confirm that the X-links themselves are not the limiting factor in the analytical payload envelope, a static structural simulation was performed in Fusion 360 on a single X-link (203 mm pin-to-pin, 3 mm aluminum 6061-T6, $E = 68.9$ GPa, $\sigma_y = 276$ MPa). The link was constrained at the center pin and at the upper roller joint, and a vertical reaction force corresponding to the worst-case lower-position load case ($F = 46.3$ N per side at $H = 28$ mm, derived from the 92.5 N total actuator force split across the two parallel X-linkages) was applied at the lower pin. The simulation predicted a peak von Mises stress of 17.6 MPa near the center pin hole, giving a yield safety factor of $n = 276/17.6 \approx 15.7$, and a maximum out-of-plane displacement of 0.19 mm, well below the 1 mm clearance allowance between the link and the rail bracket. These results confirm that the analytical capacity in Eq. (7) is governed by actuator force and joint friction rather than by link strength or stiffness within the 300–500 g prototype payload range, and that yielding or visible bending would only become a concern at loads roughly an order of magnitude above the verification cases.

Table 3: Key scissor-lift design values

Parameter	**Value**	**Meaning**
Link length	203 mm	X-link pin distance
Usable actuator range	107.5–150.96 mm	Limited by rail clearance
Measured plate height range	65–158 mm	Prototype travel: 93 mm
Estimated 7.4 V actuator speed	2.47 mm/s	Voltage-scaled value
Practical lower-position payload	0.52–0.70 kg	With $\eta = 0.6$–0.8

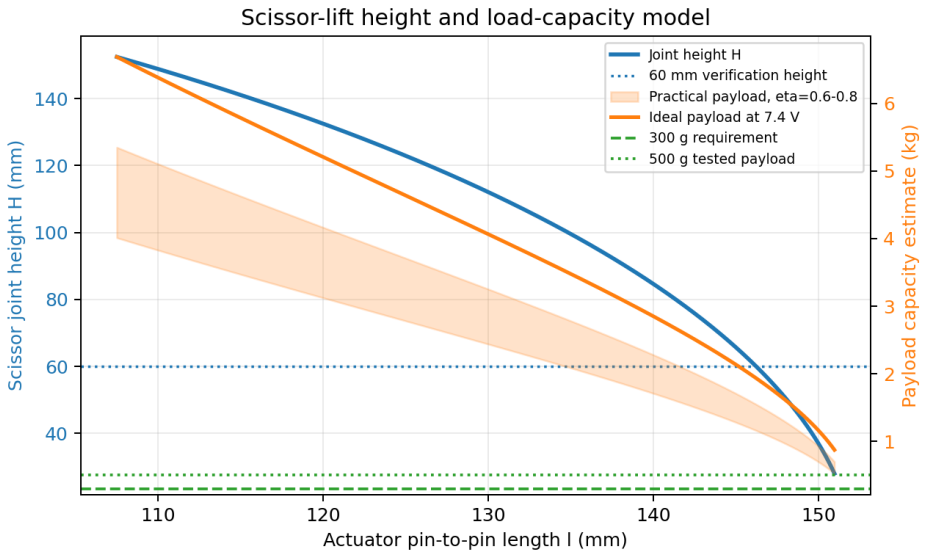

Figure 6: Calculated scissor-lift height and estimated payload capacity as a function of actuator length.

3.1.3 Deployable Side Wings

The side-wing design uses a rotary support plate instead of a linear slider. A small drive gear rotates the wing about a turntable-like joint, reducing exposed rails and allowing the support surface to fold into the platform outline (Figure 7).

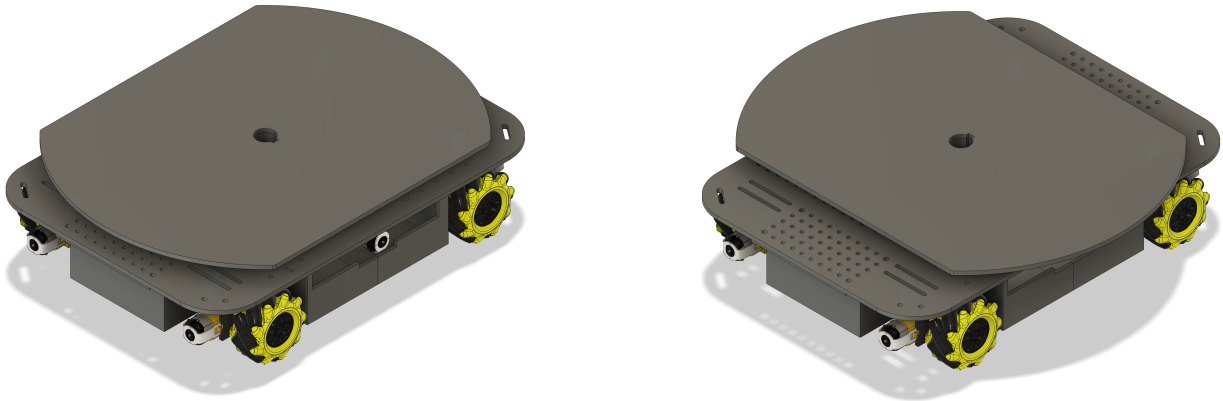

(a) Retracted state

(b) Expanded state

Figure 7: Rotary side-wing mechanism in the retracted and expanded states.

The circular support envelope has radius $R = 170$ mm, giving

$$D = 2R = 340 \text{ mm}. \tag{8}$$

The central body width is about 250 mm, and the final CAD records a 70 mm total increase in effective support width. This is reported as a CAD-level support-envelope feature rather than a verified load-bearing requirement.

The side-wing turntable plate is made from acrylic (PMMA), which is lightweight, easy to laser cut, and stiff enough for a compact support plate, but is also relatively brittle compared with aluminum. Therefore, the design check focused on stress concentration near the fixed turntable hole and deflection at the unsupported outer edge. Figure 8 shows the finite element method (FEM) result for the installed loading case: one 1.5 N downward load was applied at each side edge, while the center hole was fixed to represent the turntable mount.

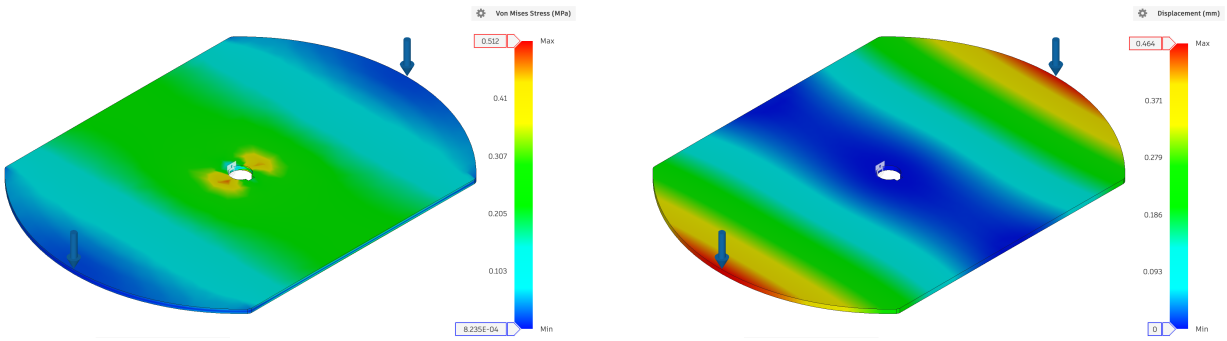

(a) Von Mises stress (b) Local displacement

Figure 8: FEM simulation of the acrylic rotary side-wing plate under two 1.5 N edge loads with the center turntable hole fixed.

The maximum von Mises stress is 0.512 MPa, concentrated near the center mounting hole, and the maximum displacement is 0.464 mm at the loaded outer edges. Since typical acrylic tensile strength is on the order of 60 MPa, the stress level is far below the material limit, and the sub-millimeter deflection is acceptable for the prototype support-envelope function.

3.1.4 Frame and Stability Check

The highest measured support-plate height was 158 mm. Taking the 250 mm body width as the minimum lateral support width gives a half-width of $b = 125$ mm. The approximate lateral acceleration required to move a centered payload projection to the support edge is

$$a_{\text{tip}} = g\frac{b}{h} = 7.76\ \text{m/s}^2. \tag{9}$$

Using the measured braking distances, the estimated braking acceleration remains below this threshold. Thus the frame is adequate for the 300–500 g prototype tests, although larger payloads would require a new support-polygon and deflection analysis.

3.2 Onboard Electronic Control System

The onboard control system bridges the BLE command path and the mechanical actuators. Figure 9 shows the prototype-level wiring schematic, including the dual battery rails, the Arduino Mega control hub, the custom L293D actuator PCB, the four commercial wheel driver modules, the HC-08 BLE module, and the common ground reference.

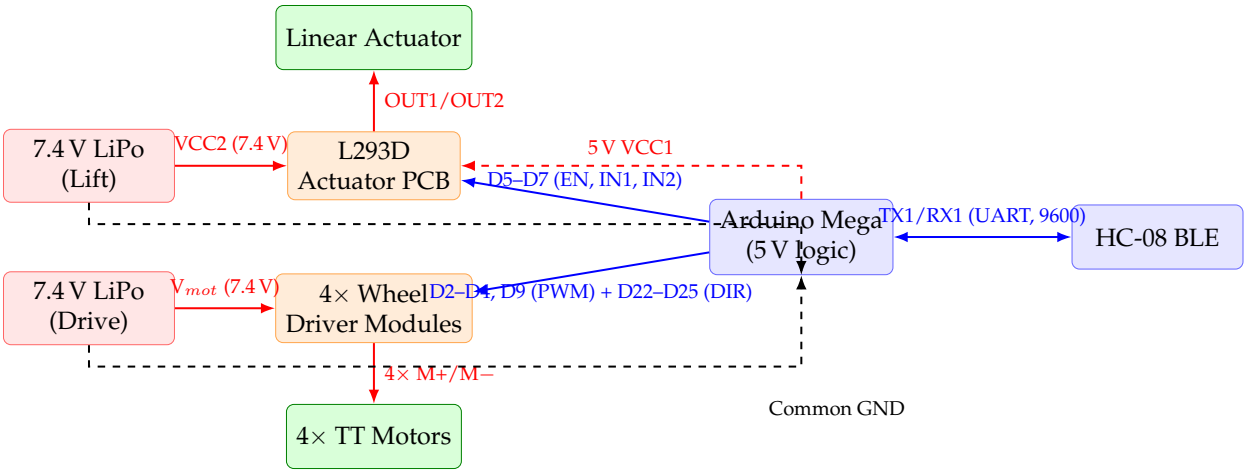

Figure 9: Prototype-level wiring schematic of the onboard electronic control system. Red solid arrows: power rails; blue solid arrows: logic-level signals; dashed: ground reference and 5 V logic supply.

3.2.1 Motor Driver PCB

The motor driver printed circuit board (PCB) was designed as a dedicated interface between the Arduino Mega control signals, the external motor power supply, and one linear actuator motor. The purpose of this PCB was to replace temporary breadboard wiring with a more reliable and organized driver circuit for the actuator used in the platform mechanism. This PCB only controls one actuator motor. The four wheel motors used for platform propulsion are controlled separately by the Arduino-based control system and are not included in this PCB design.

The PCB uses one L293D motor driver integrated circuit (IC) as an H-bridge driver. Only the left half of the L293D was used to control one direct current (DC) motor. The logic supply and motor supply were intentionally separated. Pin 16 of the L293D, labeled VCC1, was connected to the 5 V output of the Arduino Mega and served as the logic power supply for the IC. Pin 8, labeled VCC2, was connected to an external 7.4 V motor power supply and served as the motor drive supply. The external 7.4 V supply was never connected to pin 16, which protected the logic side of the L293D and the Arduino from the higher motor voltage. The Arduino ground, external battery negative terminal, and L293D ground pins, including pins 4, 5, 12, and 13, were connected to a common ground reference.

Figure 10 shows the schematic of the L293D-based motor driver PCB. The Arduino Mega provides three control signals to the driver. Pin 1 of the L293D, Enable 1/2, is connected to Arduino digital pin D5. Pin 2, IN1, is connected to D6. Pin 7, IN2, is connected to D7. The motor is connected between pin 3, OUT1, and pin 6, OUT2, instead of being connected directly between 7.4 V and ground. This connection allows the L293D to reverse the voltage polarity across the motor terminals and therefore control the actuator motor direction.

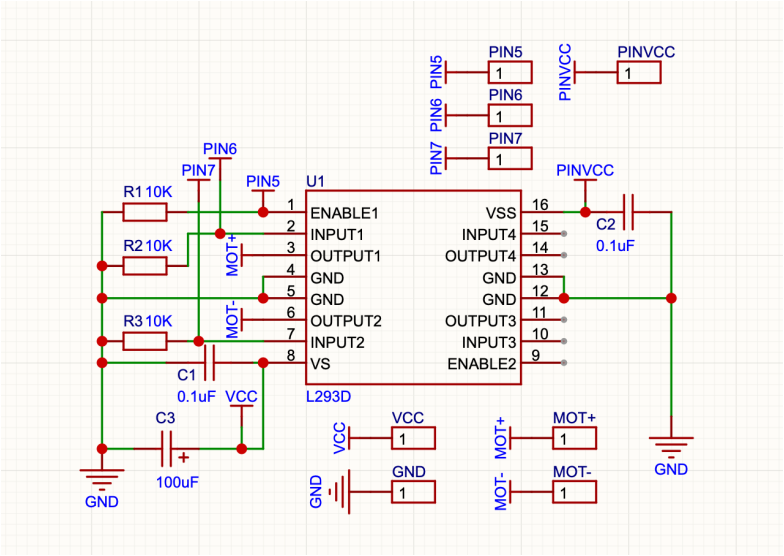

Figure 10: Schematic of the L293D-based motor driver PCB for one actuator motor.

Three 10 kΩ pull-down resistors were added to define safe default states for the driver inputs. One resistor connects Enable 1/2 to ground, one connects IN1 to ground, and one connects IN2 to ground. These resistors prevent the L293D inputs from floating during Arduino reset, startup, or temporary signal disconnection. With the pull-down resistors, the default state of the driver is disabled or stopped rather than unintentionally driving the motor.

The PCB also includes local decoupling and buffering capacitors. A 0.1 μF capacitor was placed between VCC1 and ground to reduce logic-side supply noise. A second 0.1 μF capacitor was placed between VCC2 and ground to reduce high-frequency noise on the motor supply rail. In addition, a 100 μF capacitor was connected between the 7.4 V motor supply and ground as a bulk buffer capacitor. This capacitor helps reduce voltage dips caused by motor startup and direction switching. No fuse was included in this PCB design, so current-limited bench testing and careful wiring checks were required before connecting the external motor supply.

The control logic for the actuator motor is summarized in Table 4. The Arduino receives serial commands and sets D5, D6, and D7 accordingly. When the command is `11`, the driver is enabled and the motor rotates in the forward direction. When the command is `00`, the driver is enabled and the polarity across the motor terminals is reversed, causing the motor to rotate in the reverse direction. When the command is `10`, the enable signal is set low and the L293D output stage is disabled, allowing the motor to coast to a stop. When the command is `01`, the driver remains enabled while both direction inputs are low, producing a stop or braking state.

Table 4: L293D motor driver control logic

Serial Command	D5 / Enable	D6 / IN1	D7 / IN2	Expected Motor State
`11`	HIGH	HIGH	LOW	Forward rotation
`00`	HIGH	LOW	HIGH	Reverse rotation
`10`	LOW	LOW	LOW	Output disabled, coast stop
`01`	HIGH	LOW	LOW	Stop or brake state

Figure 11 shows the PCB layout. The L293D DIP package was placed near the center of the board so that the input signals, motor outputs, and power connections could be routed clearly. The control input header is placed on the left side of the PCB, while the VCC, PINVCC, and ground connections are placed on the right side. The motor output connector is placed near the actuator motor terminals, which reduces wiring confusion during assembly. The layout separates the low-voltage logic input path from the motor output path as much as possible within the small board area.

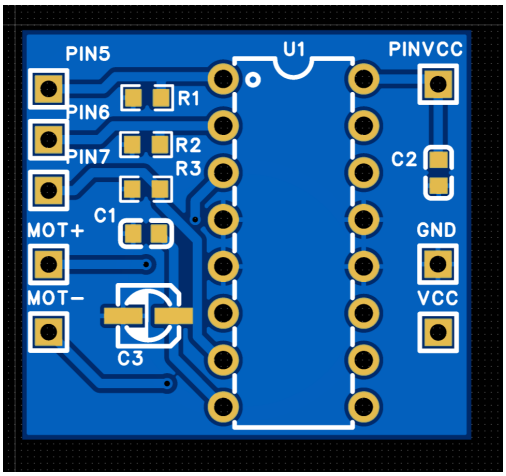

Figure 11: PCB layout of the L293D motor driver board.

Figure 12 shows the three-dimensional rendering of the assembled PCB. The through-hole DIP package and pin headers were selected to simplify soldering, debugging, and replacement during prototype development. The rendering was also used to check component placement and ensure that the capacitors, resistors, headers, and IC package did not mechanically interfere with each other.

Figure 13 shows the physical implementation of the motor driver circuit. The physical circuit was used to verify the practical wiring sequence before the final system integration. In particular, the implementation confirmed the separated 5 V logic supply and 7.4 V motor supply, the common ground connection, the pull-down resistors on Enable 1/2, IN1, and IN2, and the placement of the decoupling and bulk capacitors. This step reduced

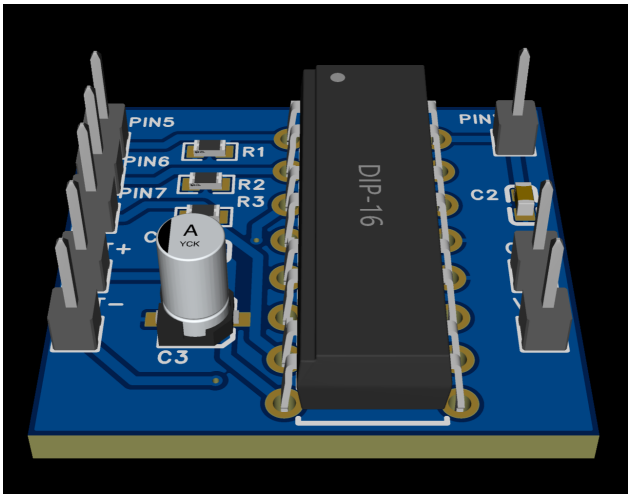

Figure 12: Three-dimensional rendering of the assembled motor driver PCB.

the risk of wiring errors when the actuator motor was connected to the Arduino control system.

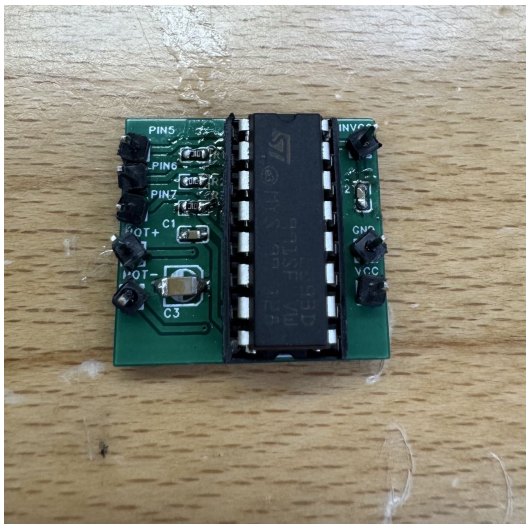

Figure 13: Physical implementation of the L293D-based motor driver circuit.

The main design limitation of this PCB is that it is intended for prototype-level actuator control rather than high-current propulsion or full-scale eVTOL handling. The L293D is suitable for small DC motor control, but its current capability and voltage drop limit its use with large motors. For this reason, the PCB was only used as a single-actuator H-bridge interface in the prototype. A future full-scale design should replace this circuit with a higher-current motor driver, add fuse protection, use wider power traces, and include a more robust connector and wiring harness.

3.2.2 Arduino & Motor driver

The Arduino Mega sits between the wireless command path and the motor drivers. It decodes incoming bytes, enforces a small safety supervisor, and drives logic-level enables and PWM outputs. Actuation is intentionally split into two hardware paths so that lift bring-up could proceed on the verified L293D PCB (Section 3.2.1) while the four corner TT gear motors remained on separate commercial driver modules during chassis testing.

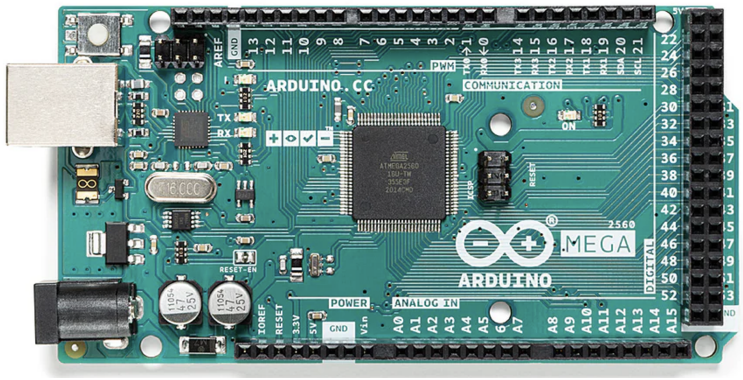

Figure 14: Arduino Mega 2560

Actuation and power architecture. The *lift path* uses digital pins D5–D7 to command Enable, IN1, and IN2 on the custom PCB; the linear actuator motor is powered from a dedicated 7.4 V pack on VCC2 while the L293D logic is fed from the Mega 5 V rail (VCC1). The *propulsion path* uses four off-the-shelf motor driver modules (Table 7) wired in a breadboard harness: each module accepts a PWM speed input and a direction or brake input from the Mega, and each TT motor is supplied from the shared low-voltage drive battery (nominal 7.4 V, compatible with the 3–9 V TT gear-motor supply range). Logic grounds for the Mega, HC-08, L293D PCB, and wheel modules are tied to a single common reference; motor return currents are routed through the driver modules rather than the microcontroller ground pins.

Table 5 summarizes the prototype power domains. A relay and panel switches listed in the bill of materials provide a manual power-cut path for bench demos; fuse protection at the battery leads is recommended before extended loaded testing but was not yet integrated into the actuator PCB.

Firmware supervisor and command paths. Firmware is structured as a periodic loop that (i) samples safety inputs first, (ii) parses new commands from `Serial1` when bytes arrive from the HC-08 link, and (iii) updates motor outputs only if the platform is not in a fault state. In IDLE, all PWM outputs are held at zero. Valid motion or lift commands transition to DRIVE, where wheel PWM and actuator direction lines are updated. An active emergency-stop input, a future limit-switch violation, or a communication timeout

Table 5: Prototype power and actuation rails

Rail / load	Nominal	Source and notes
Microcontroller logic	5 V	Mega on-board regulator from USB or external 7–12 V input; supplies HC-08 and L293D VCC1
Actuator motor (lift)	7.4 V	Dedicated pack to L293D VCC2 only; never tied to pin 16 (VCC1)
Wheel motors (4× TT)	7.4 V (shared)	Separate harness to driver modules; PWM controls average terminal voltage
Future sensors / E-stop	5 V logic	Limit switches and E-stop to digital inputs with common ground

forces FAULT, which clears PWM and disables the L293D enable line until an explicit reset sequence is received.

Two command encodings share the same Mega firmware. For **bench and USB debug**, two ASCII digits on `Serial0` map directly to the L293D control pattern in Table 4 (for example `11` forward, `00` reverse, `10` coast disable, `01` brake). For **integrated operation**, single-byte opcodes received on `Serial1` from the HC-08 are decoded into wheel PWM setpoints, rotor direction (when that motor is installed), or lift extend/retract actions; the Landing Gear page of the custom handset application issues the lift commands that ultimately assert D5–D7 through this path (Section 3.3). A placeholder communication-loss timeout of 250 ms was added in firmware so that, if no bytes arrive on `Serial1`, outputs decay to a stop condition rather than holding the last command indefinitely.

Wheel drivers and integration notes. Each commercial driver module behaves as a dual H-bridge or discrete high-current switch with logic inputs compatible with 5 V Arduino levels. The Mega sets PWM duty on the speed pins while direction pins select motor polarity; braking on the mobile base is implemented by commanding zero PWM and, where supported, asserting the driver brake or fast-decay mode rather than relying on the L293D lift PCB. Braking-distance verification on the wheeled base was performed with this wheel-driver path under stop commands issued from the operator interface; the custom L293D board was not in that current path.

The L293D datasheet absolute maximum output current per channel is 600 mA, which is adequate for the linear actuator bring-up but not for the TT propulsion motors. Keeping the lift driver on a dedicated PCB while the wheel modules handle higher transient current reduces the risk of wiring the wrong supply to the microcontroller logic rail.

3.3 Remote Control System

The remote control system uses the HC-08 BLE module as the wireless link between the operator's iPhone and the Arduino Mega. As shown in Figure 15, the module is pow-

Table 6: Arduino Mega 2560 pin assignment summary (prototype)

Function	**Pin**	**Interface**
Actuator enable (L293D EN1,2)	D5	Digital output to custom PCB
Actuator direction IN1	D6	Digital output
Actuator direction IN2	D7	Digital output
HC-08 UART TX (module RXD)	18 (TX1)	`Serial1`, 9600 baud default
HC-08 UART RX (module TXD)	19 (RX1)	`Serial1`
Wheel motor PWM (corner channels)	D2, D3, D4, D9	PWM outputs to driver modules
Wheel direction / brake (per module)	D22–D25	Digital outputs (module-dependent wiring)
Emergency stop (design)	D8	Active-low input; forces FAULT
Limit switches (planned)	D26, D27	Digital inputs for lift end-of-travel interlocks
USB debug / bench actuator test	`Serial0`	Two-digit lift commands during bring-up

ered by the Mega's 5 V rail and communicates over the hardware serial port Serial1, with HC-08 TXD connected to Mega pin 19 (RX1) and HC-08 RXD connected to Mega pin 18 (TX1).

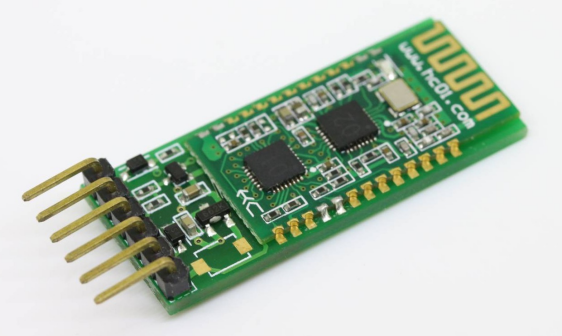

Figure 15: HC-08 BLE module.

A custom iPhone application, *eVTOL Control*, was developed in Xcode to serve as the operator interface. As shown in Figure 16, the app consists of four pages: *Drive*, which provides directional commands for ground movement; *Rotor*, which controls the rotor motor direction; *Landing Gear*, which commands the H-bridge to extend or retract the scissor lift; and *Connect*, which handles BLE scanning and device pairing. Each command is encoded as a single-byte opcode transmitted over BLE to the Mega's Serial1 interface.

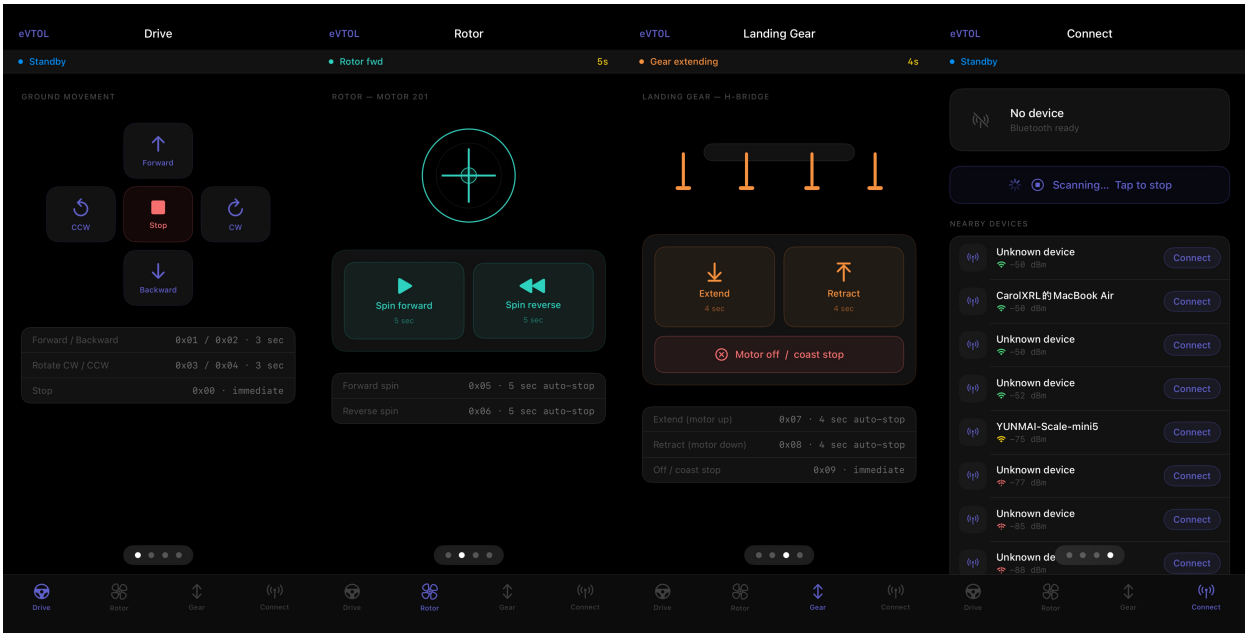

Figure 16: *eVTOL Control* app on iPhone, showing (left to right) the Drive, Rotor, Landing Gear, and Connect pages.

Future improvements include long-press continuous control and, if a vision module is integrated, autonomous docking to further reduce operator workload.

4 Verification

Table 11 in Appendix A summarizes all final requirement and verification results for the major project functions.

4.1 Mechanical Verification

This section verifies the high-level mechanical requirement: the subsystem shall lift and support a 300 g prototype payload through at least 60 mm of vertical travel within 20 s while maintaining platform stability. Detailed requirement tolerances are summarized in Appendix A.

The lift was tested on a level bench with the payload centered on the upper plate. The support plate moved from 65 mm to 158 mm, giving 93 mm of measured travel and 91 mm under the conservative ± 1 mm endpoint tolerance. With a 500 g payload, the upward full-stroke time was 23 s; scaled to the required 60 mm rise with the conservative travel bound, the worst-case time was 15.5 s. No motor stall, visible link deformation, joint binding, wheel lift, payload slip, or tip-over was observed.

The stop-command braking test produced distances from 2.2 cm to 3.0 cm over 12 trials. Including the ± 0.2 cm measurement tolerance, the worst-case distance was 3.2 cm; the prediction-bound check was 3.36 cm. Both values are below the 5.0 cm requirement. The observed no-tip behavior is consistent with the stability estimate: the centered-payload tip threshold was 7.14 $\mathrm{m/s^2}$, while the conservative braking acceleration estimate was 5.55 $\mathrm{m/s^2}$.

4.2 Onboard Electronic Control Verification

This section reports the completed test for the high-level electronic control requirement: the actuator motor driver PCB shall produce forward, reverse, and stop output states from logic-level inputs using a separated 5 V logic supply, a stable 7.4 V motor supply, and a common ground reference. Detailed low-level requirements, tolerances, and procedures are listed in Appendix A.

The L293D-based actuator driver PCB was verified on the bench before full system integration. A 5 V supply was connected to the VCC1 logic rail, a 7.4 V supply was connected to the VCC2 motor rail, and the two supplies shared a common ground. The Enable, IN1, and IN2 inputs were manually set to emulate the expected Arduino control states, and an oscilloscope measured the differential motor-terminal voltage, $V_{OUT1} - V_{OUT2}$.

The measured outputs were $+7.3$ V in the forward state, -7.2 V in the reverse state, and 0 V in the stop or disabled state. These values satisfy the Appendix A acceptance criteria: active outputs exceeded 7.0 V in magnitude, and the stop output remained within the ± 0.2 V zero-voltage tolerance. Therefore, the PCB-level electronic control requirement was satisfied. This test verifies H-bridge output polarity and voltage states; loaded actuator motion, current draw, and driver heating remain full-system integration items.

4.3 Remote Control Verification

This section reports the completed tests to satisfy high-level requirement: The remote control subsystem shall maintain a stable HC-08 BLE operator link over at least 10 m indoors and produce an operator-visible command response within 0.3 s at distances up to 10 m.

The HC-08 BLE module was tested after full system assembly on two metrics. For range, the operator stepped back and took RSSI readings at increasing distances via LightBlue. Signal strength generally decreased with distance, with localized fluctuations attributed to indoor multipath reflections; the link remained stable throughout the full test range of **60 m** with RSSI staying above -90 dBm, far exceeding the 10 m requirement in Appendix A. For latency, commands were issued repeatedly at distances up to 10 m and all responses were received within **0.3 s**, satisfying the 0.3 s response requirement.

5 Costs and Schedule

5.1 Parts Cost

Table 7 lists the final prototype bill of materials, including quantity, unit retail cost, paid cost, and source. All items were procured from Taobao, except the custom L293D actuator driver PCB, which was fabricated by JLCPCB. Retail unit prices are rounded to the nearest 10 RMB from the actual paid prices, since the team did not separately survey alternative-vendor list prices. Bulk-only or hardware items purchased by length, area, or assorted-pack (bearings, screws, adhesive, wires) are reported as a lump-sum paid cost without a meaningful unit price. Costs are reported in Chinese yuan (RMB) and converted at 1 USD = 7.2 RMB for the labor-cost comparison in the latter section.

Table 7: Final prototype bill of materials.

Item	Qty	Unit retail (RMB)	Paid (RMB)	Source
TT gear motor (150 rpm, 3–9 V)	5	20	120	Taobao
Commercial motor driver module	2	80	150	Taobao
Arduino Mega 2560 (clone)	1	220	220	Taobao
HC-08 BLE module	1	40	35	Taobao
L293D quad H-bridge IC (DIP-16)	1	20	18	Taobao
Custom L293D actuator driver PCB	1	50	50	JLCPCB
Linear actuator (12 V, 150 N)	1	90	86	Taobao
LiPo battery pack (7.4 V)	2	50	100	Taobao
Wheel + coupler (60 mm rubber)	1	120	120	Taobao
Linear guide rail	1	160	160	Taobao
Optical shaft (8 mm)	1	90	85	Taobao
Gear (rotary wing drive)	1	80	76	Taobao
Aluminum plate	1 m^2	40	40	Taobao
Acrylic plate	1 m^2	20	20	Taobao
PVC pipe (frame stock)	5 m	13	65	Taobao
Relay (5 V SPDT)	1	10	10	Taobao
Power switch	1	20	20	Taobao
Bearings (assorted)	–	–	48	Taobao
Screws (assorted)	–	–	36	Taobao
Adhesive plaster / wires (assorted)	–	–	25	Taobao
Total (paid)			**1482**	

A projected bulk-purchase cost (1000-unit batch, conservative 40% discount on commodity electronics and 25% on mechanical hardware) is approximately 1050 RMB per unit, suggesting the prototype concept is within the range of a commercial low-cost ground-handling tool if mechanical fabrication is moved to injection-molded or stamped parts.

5.2 Labor Cost Estimate

ECE 445 specifies a labor cost model per team member:

$$\text{labor cost} = (\text{ideal hourly salary}) \times (\text{actual hours}) \times 2.5. \tag{10}$$

For this project, each of the four team members was assigned 80 actual engineering hours and an ideal hourly salary of \$30.00/hour. Applying Equation 10, the estimated labor cost for each member is

$$30.00\ \text{USD}\,\text{h}^{-1} \times 80\ \text{h} \times 2.5 = 6{,}000\ \text{USD}.$$

Across Haowen Chen, Shu Yang, Ruiling Xu, and Yuchen Zhang, the total labor commitment is therefore 320 hours and the standardized ECE 445 labor estimate is \$24,000, equivalent to 172,800 RMB using the 1 USD = 7.2 RMB conversion applied in this section. This amount is reported as an engineering cost estimate rather than as an out-of-pocket project expense.

5.3 Schedule

Table 8: Project schedule with weekly task assignments.

Week	**Haowen Chen** (Mechanical)	**Shu Yang** (Mechanical)	**Ruiling Xu** (Electrical)	**Yuchen Zhang** (Electrical)
2/25	Research scissor-lift and side-wing mechanisms	Parameter calculation, component selection	Research Arduino control architecture	Research Bluetooth (HC-08) protocol
3/3	Scissor-lift and side-wing CAD modeling		Component procurement; circuit schematic design	RFA document preparation
3/10	Chassis frame and upper platform CAD	Side-wing rail assembly CAD	Breadboard stepper motor driver test	Bluetooth pairing test with smartphone
3/17	Force analysis and tolerance calculation	Stroke verification and interference check	Breadboard DC motor driver test	App Inventor remote control UI
3/24	3D-printed part design (hinge brackets, motor mounts)	Drive wheel and rail mounting bracket design	Sensor wiring (HC-SR04, limit switches)	Arduino state machine code framework
3/31	Complete full CAD assembly; Proposal & Design Doc writing		Design Doc writing (electrical sections, tolerance analysis)	
4/7	Order parts; begin 3D printing	Cut aluminum; assemble chassis frame	Design and order PCB shield	Closed-loop lift control code
4/14	Assemble scissor-lift mechanism	Assemble side-wing mechanism	Solder PCB; complete wiring	Differential drive and encoder code
4/21	Mechanical–electrical integration and joint debugging			
4/28	Full-system workflow test (lift–deploy–drive–dock)		E-stop and limit switch verification	Bluetooth full-function test
5/5	Mock Demo rehearsal; verify all R&V items and record test data			
5/12	Final Report writing (mechanical design, CAD, analysis)		Final Report writing (circuit, code, test data)	
5/19	Final Demo and presentation			

6 Conclusions, Ethics, and Broader Impacts

6.1 Accomplishments

The strongest quantitative evidence completed this term is the **bench verification of the custom L293D actuator motor driver PCB**. With the Arduino Mega disconnected, the team emulated the Enable and direction inputs using bench supplies and measured motor-terminal differential voltages of approximately $+7.3$ **V** (forward), -7.2 **V** (reverse), and 0 **V** (stop/disabled), matching the intended H-bridge output states. The board design also enforces a **separated 5 V logic supply and 7.4 V motor supply** with a common ground reference, adds **10 kΩ pull-downs** on control inputs for safe defaults, and documents decoupling and bulk capacitance behavior at the prototype level (Section 3.2.1).

Mechanically, the prototype completed the high-level lift and mobility checks reported in Section 4.1: it raised a 500 g payload through a measured 93 mm support-plate stroke, reached the required 60 mm rise within a worst-case 15.5 s, and stopped within 2.2–3.0 cm across twelve stop-command trials. The side-wing plate also stayed within the finite-element deflection estimate, with an average measured displacement of 0.417 mm under the 500 g test load.

From a project-management perspective, our team produced an updated **parts cost table** aligned with the current prototype direction (including Arduino Mega, linear actuator, HC-08 module, motors, and PCB components) and a **weekly schedule** showing parallel mechanical and electrical work streams (Table 7 and Table 8).

6.2 Uncertainties and Limitations

Table 9 summarizes the dominant remaining uncertainties with quantitative bounds. The largest unresolved electrical uncertainty is the gap between the no-load PCB output-state verification and a long-duration loaded actuator test driven through the custom PCB: the lift motion was demonstrated mechanically, but the L293D current draw and IC thermal rise were not characterized over repeated loaded cycles. Using the L293D 600 mA per-channel limit and the actuator's 12 V rated current of 0.5 A, the expected 7.4 V draw is 0.30–0.45 A, leaving 25–50% headroom—adequate for prototype use but tight enough to warrant a higher-rated driver in any follow-on revision.

Table 9: Remaining uncertainties with quantitative bounds and mitigations.

Uncertainty	Quantitative bound	Impact / mitigation
Loaded actuator current at 7.4 V	0.30–0.45 A vs. L293D 0.6 A limit (25–50% headroom)	Possible thermal derating under long lift duty; mitigate with a higher-current driver (e.g. BTS7960) in v2
Battery droop under load	LiPo sag 0.3–0.5 V at 1 C $\rightarrow$ actuator $\geq$6.9 V	$\sim$7% force reduction, inside the $\eta = 0.6$–0.8 band in Eq. (7); no design change
BLE robustness under motor noise	RSSI margin $\geq$30 dB at 10 m; $n = 12$ trials only	Small sample; mitigate with the 250 ms firmware command-timeout and extended soak tests
Braking-distance reproducibility	95% prediction bound 3.36 cm vs. 5.0 cm requirement (1.64 cm margin)	Adequate for flat indoor floor; coupling with payload shift at higher speeds not characterized

6.3 Future Work and Alternatives

Near-term engineering priorities should be: (1) repeat the loaded lift test through the verified actuator PCB while recording current draw, driver temperature, time-to-extend, and hold behavior; (2) add wheel encoders or another repeatable speed measurement method to strengthen the braking-distance dataset; (3) expand Appendix A with raw trial logs and instrumentation details for the lift, wing, mobility, and wireless tests; (4) migrate from breadboarded wheel drivers to a **robust harness or consolidated PCB** with fuse protection; (5) formalize the **HC-08** command protocol and add fail-safe behavior for loss of link.

Longer-term alternatives include replacing BLE with a purpose-built radio link if deterministic latency becomes critical, adopting a modular cradle that detaches from the chassis for maintenance, adding vision-based alignment for docking, and revisiting drivetrain topology if turning scrub or payload growth makes a non-holonomic base preferable.

6.4 Ethical Considerations and Broader Impacts

This project follows the **IEEE Code of Ethics** [3], including the obligation to be honest about claims, to disclose limitations that affect safety interpretations, and to hold paramount the safety, health, and welfare of the public.

Table 10 summarizes representative risks for this prototype class and mitigations. Even though the platform is not certified ground-support equipment, transparent reporting matters: overstating verified load or wireless reliability could mislead a reader into unsafe reuse of the design.

Broader impacts, if the concept matures responsibly, include reducing repetitive manual handling injuries, improving predictability of ground flows around eVTOL operations, and lowering avoidable airframe damage from improvised support schemes. Those benefits require follow-on validation, hazard analysis, and controls engineering beyond the current prototype scope.

Table 10: Ethical and safety considerations mapped to mitigations.

Risk category	**Mitigation and reporting practice**
Pinch/crush (scissor and moving chassis)	Guard pinch points during demos; label high-motion areas; use limit switches and controlled power levels during bring-up
Electrical energy storage	Avoid shorting packs during reconfiguration; prefer fused feeds in future revisions; document supply separation assumptions
Loss of supervisory control	Implement explicit stop defaults and command timeouts in firmware; treat wireless as bench-supervised until validated
Misrepresentation of capability	Keep Appendix A and narrative aligned; distinguish CAD, electrical bench pass, and full system demonstration

Appendices

Appendix A. Complete Requirement and Verification Table

Appendix A gives the compact requirement and verification table including both high-level requirements in Section 4 and low-level requirements. Detailed derivations and data analysis for high-level requirements and verification are discussed in Section 4.

Table 11: Complete requirement and verification table

Function	Requirement & tolerance	Verification procedure	Results
Payload capacity	Lift and support $\geq$300 g; payload tolerance $\pm$10 g.	Center payload and run one full loaded lift stroke; inspect for stall or slip.	500 g tested; lower-bound mass 490 g. Pass, margin 190 g.
Lift stroke	Vertical rise $\geq$60 mm; ruler tolerance $\pm$1 mm at each endpoint.	Measure upper-plate height at lowered and raised positions from the same base reference.	Measured 65–158 mm. Conservative travel = 91 mm. Pass, margin 31 mm.
Lift time	Required 60 mm rise within 20 s; stopwatch tolerance $\pm$0.5 s.	Record full-stroke time and scale to 60 mm using the conservative 91 mm travel.	Loaded upward stroke 23 s; worst-case $t_{60} = 15.5$ s. Pass, margin 4.5 s.
Braking distance	Stop within 5.0 cm after command; tape/front-edge tolerance $\pm$0.2 cm.	Drive across a marked trigger line, issue stop command, and record stopping distance for 12 trials.	Distances 2.2–3.0 cm; worst with tolerance 3.2 cm; prediction bound with tolerance 3.36 cm. Pass.
Platform stability	No visible deformation, joint binding, motor stall, wheel lift, payload slip, structural damage, or tip-over; payload-centering tolerance $\pm$10 mm.	Observe loaded lift and braking tests; compare estimated braking acceleration with tip-over threshold.	No failure observed. Tip threshold 7.14 m/s^2; braking estimate 5.55 m/s^2. Pass.
Side-wing displacement	Average edge displacement shall remain below the FEM estimate of 0.464 mm under the 500 g test load, approximately 2.5 N per side.	Measure both side-edge heights before and after applying the 500 g load; average the two vertical drops.	Average displacement 0.417 mm, below 0.464 mm. Pass.
PCB output states	L293D PCB shall produce forward, reverse, and stop outputs from logic inputs; active outputs accepted if $\lvert V_{OUT1} - V_{OUT2}\rvert \geq 7.0$ V, stop if within $\pm$0.2 V of 0 V.	Use 5 V logic and 7.4 V motor supplies; emulate Enable / IN1 / IN2 states and measure $V_{OUT1} - V_{OUT2}$.	Forward $+7.3$ V, reverse -7.2 V, stop 0 V. Pass.
Power rails	PCB shall keep 5 V logic and 7.4 V motor rails separate while sharing common ground.	Power VCC1 from 5 V, VCC2 from 7.4 V, tie grounds, and verify motor output responds only through H-bridge states.	Bench setup used separated 5 V/7.4 V rails with common ground; output was not directly tied to supply or ground. Pass.
BLE range	HC-08 BLE link shall remain stable beyond 10 m indoors; RSSI should stay above the observed stable threshold of -90 dBm.	Use LightBlue to record RSSI while increasing operator distance and checking connection state.	Stable through 60 m with RSSI above -90 dBm. Pass, range margin 50 m.
BLE response	Commands shall produce an operator-visible response within 0.3 s at distances up to 10 m.	Issue repeated commands at distances up to 10 m and observe response time.	All tested responses occurred within 0.3 s. Pass for operator response.

References

[1] A. P. Cohen, S. A. Shaheen, and E. M. Farrar, "Urban air mobility: History, ecosystem, market potential, and challenges," *IEEE Transactions on Intelligent Transportation Systems*, vol. 22, no. 9, pp. 6074–6087, 2021.

[2] L. A. Garrow, B. J. German, and C. E. Leonard, "Urban air mobility: A comprehensive review and comparative analysis with autonomous and electric ground transportation for informing future research," *Transportation Research Part C: Emerging Technologies*, vol. 132, p. 103 377, 2021.

[3] IEEE. "IEEE Code of Ethics," Accessed: May 8, 2026. [Online]. Available: https://www.ieee.org/about/corporate/governance/p7-8.html.